SCIENTIFIC REPORTS

OPEN

SUBJECT AREAS:
ENERGY
NANOWIRES
STRUCTURAL PROPERTIES
SOLID-STATE CHEMISTRY

Received
8 March 2013

Accepted
4 April 2013

Published
22 April 2013

Correspondence and requests for materials should be addressed to X.W. (wangxun@mail.tsinghua.edu.cn)

Nanowire Membrane-based Nanothermite: towards Processable and Tunable Interfacial Diffusion for Solid State Reactions

Yong Yang, Peng-peng Wang, Zhi-cheng Zhang, Hui-ling Liu, Jingchao Zhang, Jing Zhuang & Xun Wang

Department of Chemistry, Tsinghua University, Beijing 100084, P. R. China.

Interfacial diffusion is of great importance in determining the performance of solid-state reactions. For nanometer sized particles, some solid-state reactions can be triggered accidently by mechanical stress owing to their large surface-to-volume ratio compared with the bulk ones. Therefore, a great challenge is the control of interfacial diffusion for solid state reactions, especially for energetic materials. Here we demonstrate, through the example of nanowire-based thermite membrane, that the thermite solid-state reaction can be easily tuned via the introduction of low-surface-energy coating layer. Moreover, this silicon-coated thermite membrane exhibit controlled wetting behavior ranging from superhydrophilic to superhydrophobic and, simultaneously, to significantly reduce the friction sensitivity of thermite membrane. This effect enables to increase interfacial resistance by increasing the amount of coating material. Indeed, our results described here make it possible to tune the solid-state reactions through the manipulation of interfacial diffusion between the reactants.

Solid-state reactions are one of the most important chemical reaction categories, and have the advantages of solvent-free and low cost in material synthesis and energy generation fields[1–3]. In solid state reactions, interfacial diffusion usually determines the reaction velocity. However, condense states of the precursors are usually in irregular powder forms, which make it difficult to carefully engineer the interfacial diffusion and the subsequent chemical reaction[4–6]. Therefore, mass transport between the reactant plays a dominant role in solid-state reaction. Here, we investigate solid-state reaction based on thermite reaction from the point of view of interfacial diffusion.

Thermite reaction, a classic example of the solid-state reaction, is a self-propagating, highly exothermic reaction. Recently, thermite reaction has been gaining intense research due to the great potential for practical use in civilian purposes, particularly in micro-electromechanical systems (MEMS)[7–9]. Significant progress has been made in the synthesis of various thermite composites[10–12]. For instance, some thermite composites composed of micrometer-sized particles feature the large diffusion distance between fuel and oxidizer. With the development of materials engineering and science, these considerations can be changed or eliminated by using different assembly technology[13,14]. The self-assembly strategy has great advantages in the synthesis of advanced functional materials[15–17]. In the present work, we introduce aluminum nanoparticles into one dimension-based membrane to prepare novel thermite membrane based on the electrostatic interaction and self-assembly. This fabrication method presents a way to maximally decrease the diffusion distance and increase intimate contact. Given that most of solid-state reactions were heterogeneous, the reaction velocity of solid-state reaction was governed by the heat conduction and interfacial diffusion. For instance, reduced-sensitivity MnO_2/Al thermite can be obtained by enclosing metal oxide inside carbon nanofibers[18]. Therefore, spatial distribution between reactants and surface modification are supposed to be an alternative way to influence interfacial diffusion[19–21]. Here, the friction of thermite membranes can be manipulated by adjusting the interfacial diffusion to influence the thermite solid-state reaction. Moreover, functional surface silicon coatings not only can change the wetting behavior of thermal thermite membrane from superhydrophilic to superhydrophobic resulting in the long-time stability, but also can be regarded as "sheath" that increases interfacial resistance between the oxide and fuel. Friction sensitivity studies reveal that there was a dramatic reduction for the silicon-coated thermite membrane as compared to the pristine thermite membrane (less than < 5 N). Furthermore, this assembly method can be

applied to prepare CuO/Al thermite membrane. This thermite membrane possess robust and portable property with a tunable friction sensitivity, which makes it them as new energetic materials.

Results

Figure S1 describe the fabrication process of free-standing thermite membrane. This novel and flexible thermite membrane can be obtained after simple suction filtration. A typical sample of the thermite membrane with square shape is shown in Figure 1a. The shape of thermite membrane can be easily manufactured according to the specific demand. A scanning electron microscopy (SEM) image in Figure 1b shows a cross sectional view of the nanowire membrane consisting of many randomly oriented nanowires, which are interconnected and assembled with each other. We hypothesize that the excellent mechanical flexibility attributes to this mutual involvement. The average size of the original aluminum nanoparticles was about 80 nm (Figure S2). Each aluminum nanoparticle was covered by about 3 nm thick amorphous alumina passivation layer (Figure 1c). The passivation oxide shell will account for a significant content for nano-scale aluminum and has a critical impact on the behavior of the thermite reaction (Supporting Information Figure S3)[22]. Taking into consideration the hydration of aluminum, the time of exposure in the water should be limited. In addition, $NH_4H_2PO_4$ was added into the aqueous solution as an inhibitor[23]. There was no obvious deterioration for passivation layer after in aqueous solution with the help of the $NH_4H_2PO_4$ (Supplementary Information, Figure S4). Figure 1c–d shows the low- and high-magnification TEM image of the MnO_2 nanowires. The lattice fringes is the {110} and {400} with a d-spacing of 0.23 nm and 0.25 nm, respectively. It is expected that aluminum nanoparticles can be closely packed into this nanowire-based membrane. The three dimensional assembly clearly displays interpenetrating nanowire networks with aluminum nanoparticle (Fig. 1f).

One of the unique advantages of the self-assembled thermite membrane was a water-based method rather than pure organic solution method such as isopropanol. Hydrogen bond plays a critical role in the formation of this network membrane in aqueous solution because MnO_2 nanowires obtained by hydrothermal method were highly functionalized with hydroxyl groups[24,25]. In order to improve dispersion and intimate contact of reactants in aqueous solution, the

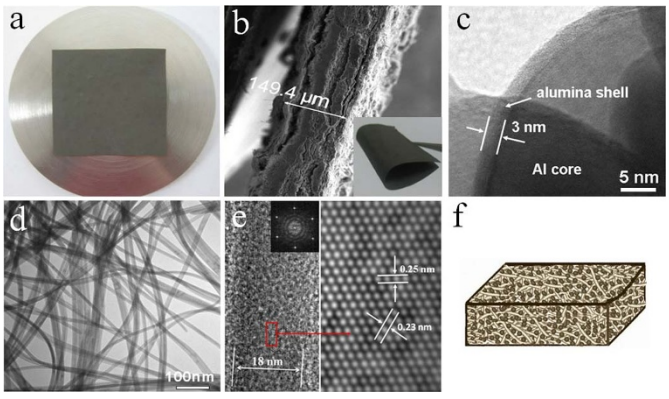

Figure 1 | (a) Optical image of the as-obtained thermite membrane (dimensions 5 cm × 5 cm × 0.1 mm) containing MnO_2 nanowires and aluminum nanoparticles after vacuum filtration. (b) SEM image of cross-sectional area of the thermite membrane, showing a layered structure. The inset image demonstrates the flexibility of the thermite membrane. (c) High-magnification TEM image of aluminum nanoparticles shows amorphous passivation alumina layer. (d) The TEM image of the MnO_2 nanowires. (e) High-magnification TEM image of MnO_2 nanowires and the corresponding auto-correction images. (f) The three dimensional schematic diagram of the thermite membranes.

MnO_2 nanowires were modified to get positively charged by a long-chain polyelectrolyte PDDA (Figure 2a)[26,27]. Thus, the surface of PDDA-modified MnO_2 nanowires featured with positively charged will capture negatively charged aluminum nanoparticles by electrostatic attraction (Figure 2b). The SEM image of thermite membrane in figure S5 confirms the electrostatic assembly that can greatly improve the distribution of aluminum nanoparticles. For pure MnO_2 nanowire membrane, there was a pore size distribution centered about 18 nm (Figure S6). However, pore size distribution curve was smooth after adding aluminum nanoparticles, indicating that aluminum nanoparticles have packed into these pore structure. Elemental mapping spectrum in Figure 2c was carried out to investigate the interior distribution of components. These results confirm that aluminum nanoparticles are well embedded in the nanowire-based membrane. There is no doubt that this bottom-up assembly will not only drastically decrease the diffusion distances and transport limitation and increase the number of contact points between the reactants, but also will prevent the oxidation of aluminum. The thermite membrane with different equivalence ratio can be tailored by adding the different amount of aluminum nanoparticles (see Table 1 for more details).

To realize the modification of thermite membrane, we employed a simple vapor deposition technique to coat a low-surface-energy layer[20]. The MnO_2 nanowires and aluminum nanoparticles are uniformly coated with a layer with thickness up to several nanometers (Supplementary Information, Figure S7). Compositional analysis of this layer reveals the presence of silicon and oxygen by energy-dispersive X-ray spectroscopy (Figure S8). Fourier transforms infrared (FTIR) spectroscopy indicates the presence of SiO and CH_3-Si group (Figure S9). These volatile silicon molecules will deposit and subsequently crosslink on the surface of the thermite membrane, leading to change the surface wetting property of the membrane. Interestingly, the superhydrophobic and superhydrophilic behavior of thermite membrane can be changed at elevated temperatures by removing this hydrophobic molecule (Figure 3a). This means that silicone coated layer with functional hydrophobic groups will be released during the thermite reaction. Figure 3b shows the relationship between pH and water contact angle on the superhydrophobic membrane surfaces. There was no noticeable change of the water contact angle over the pH range from 1 to 14 (more than 150°). Notably, the superhydrophobicity of the silicone-coated thermite membrane remains essentially constant after 3 months of storage in air. It is expected that this coating layer can significantly prevent the aging process so as to increase shelf-life. The atomic force microscopy topography image in Figure 4a clearly shows that there were many pores on the surface of thermite membrane with highly rough structure. Stress-strain curves (Figure 4b) show that silicon-coated thermite membrane becomes more fragile than pristine thermite membrane. This observation is expected owing to the PDMS heat treatment (Supplementary Information, Figure S10). It should be noted that the superhydrophobicity of the silicone-coated membrane remains unaltered after being immersed in water (Figure 4c–e and Supplementary Video), which shows full silicon coating on surface coverage throughout both sides of the thermite membrane. In addition, thermal properties of the thermite membrane were characterized by differential scanning calorimeter (Supplementary Information, Fig. S11). The heat of reaction was lower than the theoretical values, we hypothesize that this result from an alumina passivation layer as well as the silicon coating layer.

Discussion

These silicon-containing layers with functional hydrophobic group can not only create a low-energy surface, but also reduce friction sensitivity of thermite membrane. According to the international standards, the product is not allowed to be transported on public roads if the friction sensitivity is below 80 N[28,29]. Friction sensitivity

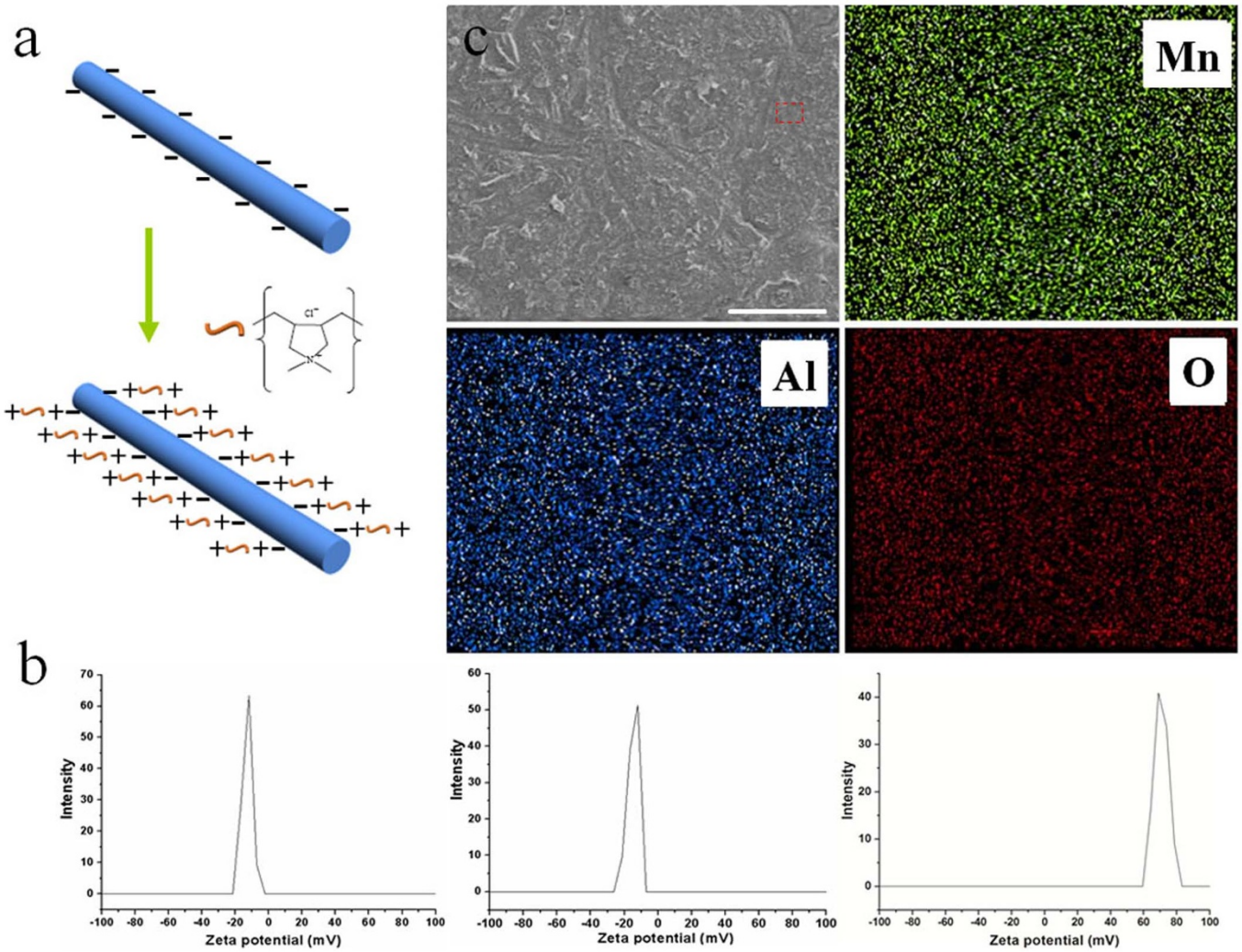

Figure 2 | (a) Illustration of charge transformation process for MnO_2 nanowires by PDDA and the chemical structure of PDDA. (b) Zeta potential of the MnO_2 nanowires, aluminum nanoparticles and PDDA modified MnO_2 nanowires (from left to right). (c) Low-magnification SEM image of the as-obtained thermite membrane. Scale bars, 100 μm. Elemental mapping taken form the red square show the homogeneous distribution of the aluminum nanoparticles.

of pristine thermite membrane was less than 5 N. It is extremely necessary to increase the safety of energetic materials allowing for practical application. In order to investigate the relation of the silicon coatings and friction sensitivity, control experiments for thermite membrane were carried out. TEM images show that with the increase of PDMS treatment time, the thickness of SiO-containing layer increases (Figure 5a–c). Figure 5d shows the relation of PDMS treatment and friction sensitivity of MnO_2/Al thermite membrane. There was a dramatic decrease in the friction sensitivity from less than 5 N to 240 N with increasing amount of coating materials (Figure 5e), leading to moderately sensitive products. Therefore, this silicon-coating layer has a significant influence on interfacial diffusion between the reactants.

Friction occurs during sliding contact of reactants alone with the transformation of energy. Friction is usually converted into heat, which raises the interface temperature in turn. According to the hot spot theory[30,31], local temperature will heat up and reach a certain temperature. Then molten aluminum will spurt and initiate the thermite reactions as the alumina barrier rupture. In this silicon coated nanothermite membrane, fuel and oxidizer were separated by alumina and silicon coating layer. It is logical to assume that the presence of silicon coating layer as a barrier hinders effectively the

Table 1 | Characteristics of MnO_2/Al thermite membrane with different equivalence ratio

Sample	n-Al (g)	MnO_2 Nano-wire (g)	Active aluminum mass faction† (Wt%)	Active aluminum mass faction‡ (Wt%)	MnO_2 oxidizer mass§ (Wt%)	TMD* (g/cm^3)	Ø
S1	0.026	0.04	25	14.5	60.5	4.294	1
S2	0.031	0.04	27.6	16.9	56.4	4.253	1.2
S3	0.036	0.04	30.3	17.5	52.2	4.139	1.4

†Fraction of active aluminum in the total composites. Active aluminum content is determined from thermo-gravimetric analysis (Supplementary Fig. S3). ‡ Fraction of alumina mass in the total composites.§Fraction of oxidizer mass in the total composites. *The theoretical maximum densities (TMD) is defined as a mixture with no voids and a density equal to that of the densities of its component parts multiplied by their respective mass ratios. The ratio of fuel to oxidizer (Ø) is defined as the fuel stoichiometric coefficient.

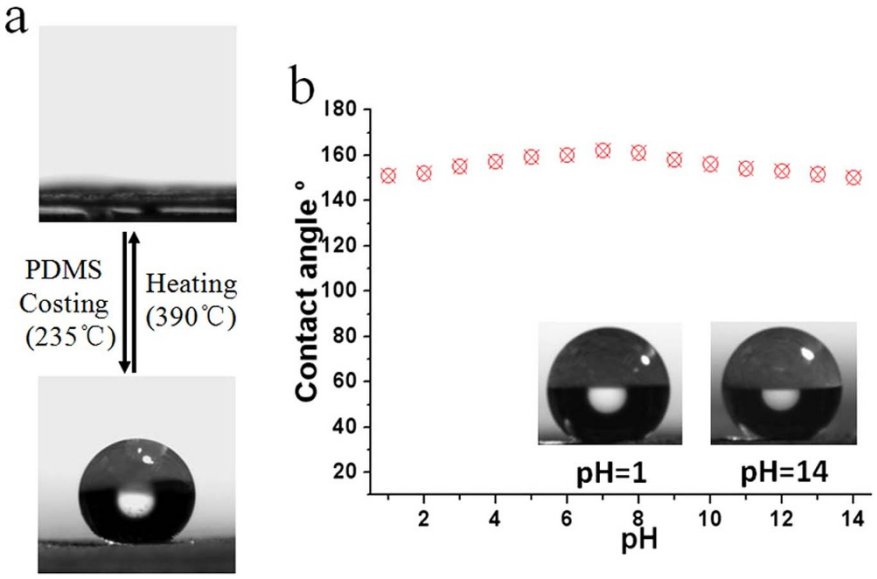

Figure 3 | (a) Representation of the reversible transition between superhydrophilic (top) and superhydrophobic (bottom) states of the nanothermite membrane. (b) The relationship between a series of pH and contact angle on the superhydrophobic surfaces. Inset: video snapshots of a water droplet on the membrane with pH 1 and 14, respectively.

thermal diffusion so as to prevent the generation of hot spots to some extent. To further examine condensed-phase reaction during the initiation of thermite reaction, interfacial diffusion between fuel and oxidizer was simplified as an infinite plate model. An illustration of this is shown in Figure 5f, a formula of the thickness of silicon coating layer with temperature difference is derived (Details can be found in Supporting Information Figure S12). $S = \frac{\Delta t}{Q}\lambda A$ Where S is the thickness of silicon coating layer, Q is the resistance of thermal diffusion, λ is the thermal conductivity of silicon coating layer, A is the area of silicon coating layer, Δt is temperature difference caused by friction. For pristine thermite membrane, $\lambda \rightarrow 0$ and $S \rightarrow 0$, hot spot can easily generate during friction without being any impeded. For silicon-coated thermite membrane, λ increases, leading to more obstacles. The thicker silicon coating layer was, the harder it was for heat caused by friction to pass this inert layer. The threshold to initial the thermite reaction was proportional to the thickness of silicon coating layer. For micrometer-sized aluminum, given that the high ignition temperature and the high burn pressure compared with nano-sized aluminum, we suspect that it is difficult to initiate the reaction. Experimental result shows that the friction sensitivity was higher than 360N using micro-sized aluminum, leading to completely insensitive products (Supporting Information Figure S13). These results show that the introduction of inert molecular layer leads to a considerable reduction in the friction sensitivity. The thicker silicon coating layer means more resistance during interfacial thermal diffusion.

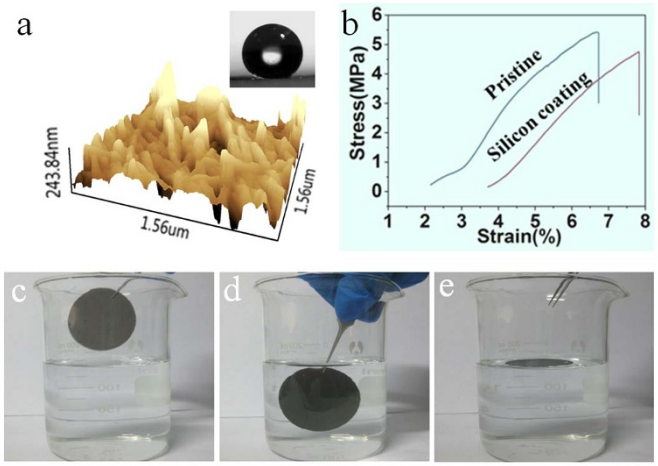

Figure 4 | (a) Three-dimensional AFM appearance of thermite membrane surfaces. The inset shows typical water contact angle measurements of the silicone-coated thermite membrane. (b) Stress-strain curves for pristine thermite membrane and silicone-coated thermite membrane made based on the S2 composition. (c–e) Photographs of the silicone-coated thermite membrane immersed in water remain unaltered its wetting behavior.

To further examine the thermite reaction, the reaction residues were collected for the X-ray diffraction analysis (Figure S14). Manganosite is formed by reoxidation of the formed manganese metal with oxygen due to fierce exothermic reaction. The presence of alumina shows that aluminum and MnO_2 reacted as mentioned the reaction 3 in supporting information. Moreover, these results are not limited to MnO_2/Al thermite membrane, but are expected to apply to other free-standing thermite membrane. Nanobelts CuO/Al thermite membrane was obtained through this assembly strategy. It is found that this simple silicon coating method is a viable technique to tune the friction sensitivity of CuO/Al thermite membrane (Details can be found in Supporting Information Figure S15). A potential property of the silicone coated thermite membrane is the release of gas during the thermite reaction, which may enhance the combustion front velocity. Other characteration need to further quantitative verification.

In summary, we demonstrate the electrostatic interaction-based, bottom-up fabrication methods to prepare a novel thermite membrane with tunable friction sensitivity performance. This achievement of thermite membrane attributes to the hydrogen bond nanoscale networks in an aqueous environment. The introduction of silicon coating molecular layer exhibit controlled wetting behavior ranging from superhydrophilic to superhydrophobic and, as an obstacle, to significantly reduce friction sensitivity of thermite membrane. This effect enables to increase interfacial resistance with the help of coating materials. The present work presents a way to desensitize other dangerous energetic materials. Remarkably, the versatility of the present assembly strategy allows us to easily achieve the synthesis of other thermite membrane. This portable membrane-based

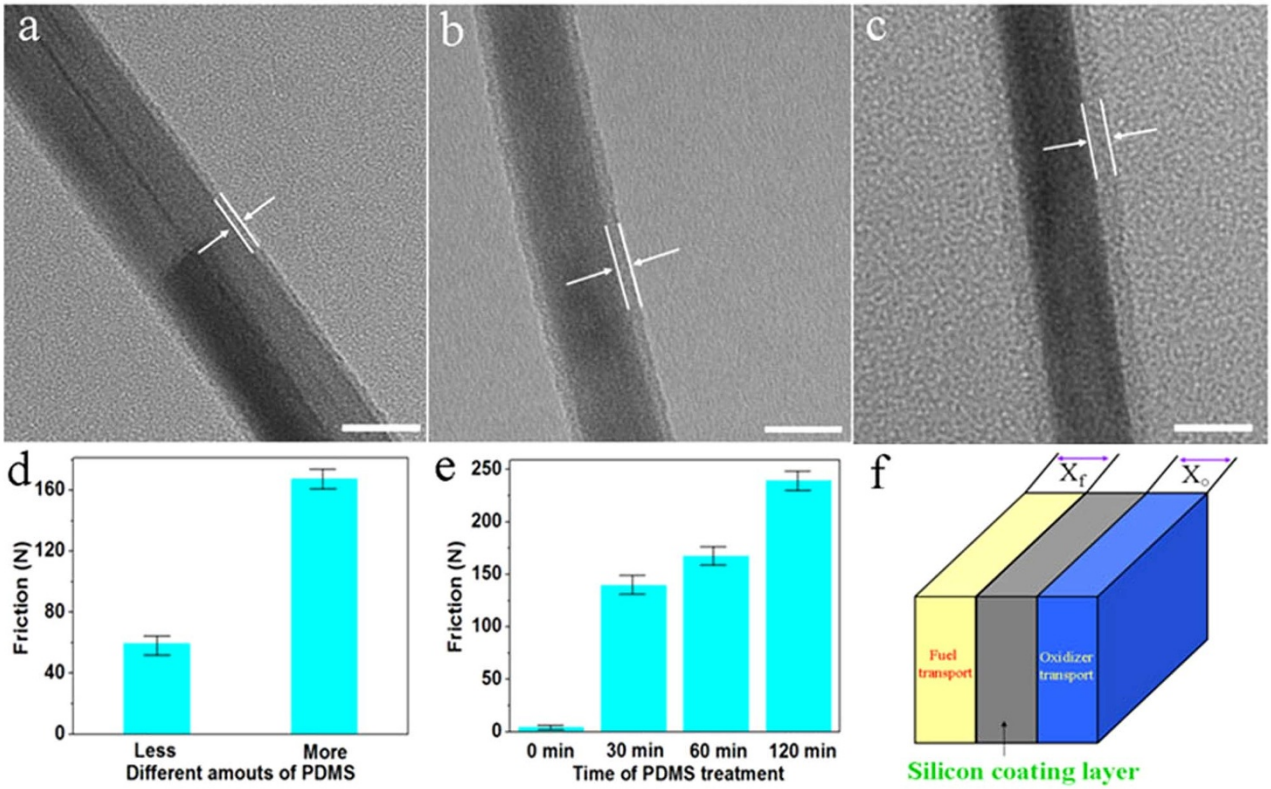

Figure 5 | (a–c) TEM image of thermite membrane coated with SiO-containing layer with different treatment time (from left to right): 30, 60, and 120 minutes, respectively; scale bar 20 nm. (d) The friction sensitivity of thermite membrane prepared at different amounts of PDMS stamp. (e) The friction sensitivity of thermite membrane prepared at different PDMS treatment time. (f) Diagram illustration of the spatially distribution of reactants. Here, the aluminum and MnO_2 nanowires were simplify to be uniformly sheets with certain thickness of X_f and X_o.

nanothermite should have practical applications in the design of next portable and safe energetic materials.

Methods

Synthesis of α-MnO_2 nanowires. Ultra-length α-MnO_2 nano-wire was synthesized using a hydrothermal method[32]. The precursor materials were composed of manganese sulphate monohydrate ($MnSO_4.H_2O$), ammonium per sulfate ($(NH_4)_2S_2O_8$), and ammonium sulfate $(NH_4)_2SO_4$ in a molar ratio of 1:1:3 in 36 ml of distilled water. The mixture was continuous stirred at room temperature to form a transparent solution and transferred to a Teflon vessel held in a stainless steel vessel. The sealed vessel was placed in an oven and heated at 180°C for 12 h. The product was washed with water a couple of times to remove impurities.

Synthesis of CuO nanobelts. The synthesis of CuO nanbelts is prepared by a simple wet chemical method[33]. In the typical experiment, 178.48 mg $CuCl_2$ were dissolved in 200 mL H_2O with a magnetic stirrer. Then, 1.2 mL of 6 M NaOH was added dropwise into the $CuCl_2$ solution keeping stirring. A blue precipitate of $Cu(OH)_2$ was soon produced. The $Cu(OH)_2$ precipitate gradually turned into a black color and aged at 90°C for 1 h. The colloid solution was centrifuged and washed with deionized water.

Preparation of the PDDA-modified α-MnO_2 NWs and stable aluminum nanoparticles solution. PDDA was added to α-MnO_2 nanowires suspension solution by vigorously stirring for 30 min to ensure the PDDA absorbed on the surface of nanowires. Excess PDDA was subsequently removed and decanted from the solution by centrifugation at 5000 rpm (5 min). Aluminum nanoparticles were dispersed and stabilized in $NH_4H_2PO_4$ aqueous solution, and the colloids were sonicated using a Uibra-cell ultrasonic probe system at 150 W for 1.5 min, with 5s pulses separated by 5 s. The aluminum nanoparticles used in this work was purchased from Beijing Nachen S&T Ltd. It is worth to note that the aluminum nanoparticles were stable in $NH_4H_2PO_4$ (0.1 Wt%) aqueous water over several weeks, whereas the particles were oxidized and disappeared in a few days when dispersed in liquid water. Therefore, ammonium dihydrogen phosphate is a very effective inhibitor of the hydration of aluminum nanoparticles.

Preparation of the thermite membrane silicone coating procedure. The PDMS coating of the thermite membrane was performed through a simple vapour deposition technique[20]. In a typical experiment, a thermite membrane and a freshly prepared PDMS stamp were placed together in a sealed glass container heated 235°C for some time and then allowed to cool to room temperature naturally. The thermal degradation of PDMS through heterolytic cleavage of the Si–O bonds leads to a mixture of volatile, low-molecular-weight products that form a conformal layer on the surface of the thermite membrane. The silicone coated nanowire-based membrane exhibited a water contact angle of more than 150°.

1. Stein, A., Keller, S. W. & Mallouk, T. E. Turning down the heat-design and mechanism in solid-state syntheis. *Science* **259**, 1558–1564 (1993).
2. Jansen, M. A concept for synthesis planning in solid-state chemistry. *Angew. Chem., Int. Ed.* **41**, 3746–3766 (2002).
3. Wiley, J. B. & Kaner, R. B. Rapid solid-state precursor synthesis of materials. *Science* **255**, 1093–1097 (1992).
4. Maier, J. Defect chemistry: composition, transport, and reactions in the solid state; part I: thermodynamics. *Angew. Chem. Int. Ed.* **32**, 313–335 (1993).
5. Maier, J. Defect chemistry: composition, transport, and reactions in the solid state; part II: Kinetics. *Angew. Chem. Int. Ed.* **32**, 528–542 (1993).
6. Khawam, A. & Flanagan, D. R. Solid-state kinetic models: basics and mathematical fundamentals. *J. Phys. Chem. B.* **110**, 17315–17328 (2006).
7. Higa, K. T. Energetic nanocomposite lead-free electric primers. *J. Propulsion Power.* **23**, 722–727 (2007).
8. Armstrong, R. W., Baschung, B., Booth, D. W. & Samirant, M. Enhanced propellant combustion with nanoparticles. *Nano Lette.* **3**, 253–255 (2003).
9. Martirosyan, K. S., Wang, L., Vicent, A. & Luss, D. Nanoenergetic gas-generators: design and performance. *Propellants, Explos. Pyrotech.* **34**, 532–538 (2009).
10. Tillotson, T. M. *et al.* Nanostructured energetic materials using sol-gel methodologies. *J.Non.Cryst. Solids.* **285**, 338–345 (2001).
11. Rossi, C. *et al.* Nanoenergetic materials for MEMS: A review. *J.Microelectromech.Syst.* **16**, 919–931 (2007).
12. Yen, N. H. & Wang, L. Y. Reactive metals in explosives. *Propellants, Explos. Pyrotech.* **37**, 143–155 (2012).
13. Severac, F., Alphonse, P., Esteve, A., Bancaud, A. & Rossi, C. High-energy Al/CuO nanocomposites obtained by DNA-Directed assembly. *Adv. Funct. Mater.* **22**, 323–329 (2012).
14. Kim, S. H. & Zachariah, M. R. Enhancing the rate of energy release from nanoenergetic materials by electrostatically enhanced assembly. *Adv.Mater.***16**, 1821–1825 (2004).

15. Cheng, Q., Li, M., Jiang, L. & Tang, Z. Bioinspired Layered Composites Based on Flattened Double-Walled Carbon Nanotubes. *Adv.Mater.* **16**, 1821–1825 (2004).
16. Wang, J., Cheng, Q. & Tang, Z. Layered nanocomposites inspired by the structure and mechanical properties of nacre. *Chem. Soc. Rev.* **41**, 1111–1129 (2012).
17. Tang, Z. Y., Kotov, N. A., Magonov, S. & Ozturk, B. Nanostructured artificial nacre. *Nat.Mater.* **2**, 413–2418 (2003).
18. Siegert, B., Comet, M., Muller, O., Pourroy, G. & Spitzer, D. Reduced-Sensitivity Nanothermites Containing Manganese Oxide Filled Carbon Nanofibers. *J. Phys. Chem. C.* **114**, 19562–19568 (2010).
19. Erbil, H. Y., Demirel, A. L., Avci, Y. & Mert, O. Transformation of a simple plastic into a superhydrophobic surface. *Science* **299**, 1377–1380 (2003).
20. Yuan, J. *et al*. Superwetting nanowire membranes for selective absorption. *Nature Nano.* **3**, 332–336 (2008).
21. Guo, Z. G., Zhou, F., Hao, J. C. & Liu, W. M. Stable biomimetic super-hydrophobic engineering materials. *J. Am. Chem. Soc.* **127**, 15670–15671 (2005).
22. Firmansyah, D. A. *et al*. Microstructural behavior of the alumina shell and aluminum core beforeand after melting of aluminum nanoparticles. *J. Phys. Chem. C.* **116**, 404–411 (2011).
23. Puszynski, J. A., Bulian, C. J. & Swiatkiewicz, J. J. Processing and ignition characteristics of aluminum-bismuth trioxide nanothermite system. *J. Propul. Power.* **23**, 698–706 (2007).
24. Long, Y. *et al*. Hydrogen bond nanoscale networks showing switchable transport performance. *Sci. Rep.* **2**, 612–612 (2012).
25. Yuan, J., Laubernds, K., Villegas, J., Gomez, S. & Suib, S. L. Spontaneous formation of inorganic paper-like materials. *Adv. Mater.* **16**, 1729–1732 (2004).
26. Zhang, S., Shao, Y., Yin, G. & Lin, Y. Electrostatic self-assembly of a Pt-around-Au nanocomposite with high activity towards formic acid oxidation. *Angew. Chem. Int. Ed.* **49**, 2211–2214 (2010).
27. Wang, S., Yu, D. & Dai, L. Polyelectrolyte functionalized carbon nanotubes as efficient metal-free electrocatalysts for oxygen reduction. *J. Am. Chem. Soc.* **133**, 5182–5185 (2011).
28. Ramaswamy, A. L. Mesoscopic approach to energetic material sensitivity. *J. Energetic Mat.* **24**, 35–65 (2006).
29. Siegert, B., Comet, M. & Spitzer, D. Safer energetic materials by a nanotechnological approach. *Nanoscale.* **3**, 3534–3544 (2011).
30. Klapoetke, T. M., Krumm, B., Steemann, F. X. & Steinhauser, G. Hands on explosives: Safety testing of protective measures. *Safety Science.* **48**, 28–34 (2010).
31. Heijden, V. D. *et al*. Modification and characterization of (energetic) nanomaterials. *J. Phys. Chem. Solids.* **71**, 59–63 (2010).
32. Wang, X. & Li, Y. Selected-control hydrothermal synthesis of α- and β-MnO_2 single crystal nanowires. *J. Am. Chem. Soc.* **124**, 2880–2881 (2002).
33. Wang, W. Z. *et al*. Synthesis and characterization of Cu_2O nanowires by a novel reduction route. *Adv.Mater.* **14**, 67–69 (2002).

Acknowledgements

This work was supported by NSFC (91127040, 21221062), and the State Key Project of Fundamental Research for Nanoscience and Nanotechnology (2011CB932402).

Author contributions

Y. Y. carried out the experimental work, analyzed the data and wrote the paper. P .P. W., Z. C. Z., H. L. L., J. C. Z. and J. Z. helped with the design and experiments. X. W. conceived the whole experimental project, analyzed the data and wrote the paper.

Additional information

Supplementary information accompanies this paper at http://www.nature.com/scientificreports

Competing financial interests: The authors declare no competing financial interests.

How to cite this article: Yang, Y. *et al*. Nanowire Membrane-based Nanothermite: towards Processable and Tunable Interfacial Diffusion for Solid State Reactions. *Sci. Rep.* **3**, 1694; DOI:10.1038/srep01694 (2013).